Distributed Hybrid-Electric Propulsion Benefits for Span-Limited Aircraft

Bonnin, V.O.; Hoogreef, M.F.M.; de Vries, R.

DOI
10.2514/6.2023-2098

Publication date
2023

Document Version
Final published version

Published in
AIAA SciTech Forum 2023

AIAA SciTech Forum
23-27 January 2023, National Harbor, MD & Online
AIAA SCITECH 2023 Forum

10.2514/6.2023-2098

Distributed Hybrid-Electric Propulsion Benefits for Span-Limited Aircraft

Vincent O. Bonnin * and
Delft University of Technology, Faculty of Aerospace Engineering, Delft, the Netherlands

Reynard de Vries †
Panta Holdings B.V., Mijdrecht, the Netherlands

Maurice F.M. Hoogreef ‡
Delft University of Technology, Faculty of Aerospace Engineering, Delft, the Netherlands

The impact of the ICAO code C gate span limit is assessed on the sizing of a serial Hybrid-Electric Aircraft (HEA) of increasing Degree of Hybridization (DoH). For a set of Top Level Aircraft Requirements (TLARs) similar to the ATR-42, it is shown that the increase in MTOM due to the presence of the battery is such that only a maximum DoH under 30% can be achieved before the wing span of the serial HEA reaches the 36 meters gate size. The same aircraft is fitted with Leading Edge Distributed Propulsion (LEDP) to increase the wing loading and relieve the span constraint, though this introduces limitations regarding the available wing volume. It is shown that a combination of high wing loading and of low volumetric energy density for batteries compared to jet fuel can lead to the available wing volume being too small for the required volume of the energy carriers. Finally a value in wing loading is found which simultaneously meets the span and wing-volume constraints. The higher DoH enabled by LEDP leads results in a 33% reduction in fuel burn compared to the fuel-based reference aircraft, while the overall energy consumption is increased by 6%.

Nomenclature

Latin Symbols

AR	=	Aspect ratio (∼)
C_D	=	Drag coefficient (∼)
C_L	=	Lift coefficient (∼)
P	=	Power (W)
T	=	Thrust (N)
S	=	Wing area (m^2)
V	=	Volume (m^3)
W	=	Weight (N)
b	=	Span (m)

Greek Symbols

ξ	=	Gas turbine throttle (∼)
Φ	=	Battery supply power ratio (∼)

Acronyms

DHEP	=	Distributed hybrid electric propulsion
DoH	=	Degree of hybridization
HEP	=	Hybrid electric propulsion
HT	=	Horizontal tail
ISA	=	International standard atmosphere
KPI	=	Key performance indicator
LEDP	=	Leading-edge distributed propulsion
MLM	=	Maximum landing mass
MTOM	=	Maximum take-off mass
OEI	=	One engine inoperative
OEM	=	Operational empty mass
SL	=	Sea-level
T/O	=	Take-off
PREE	=	Payload range energy efficiency
SMR	=	Short-medium range
TLARs	=	Top level aircraft requirements
TMS	=	Thermal Management System
VT	=	Vertical tail

*Post-Doctoral Fellow, Flight Performance and Propulsion, Kluyverweg 1, 2629HS Delft, v.o.bonnin@tudelft.nl
†Program Manager New Aircraft Technologies, Rendementsweg 2, 3641SK Mijdrecht, reynarddevries@panta-holdings.nl , AIAA Member
‡Assistant Professor, Flight Performance and Propulsion, Kluyverweg 1, 2629HS Delft, m.f.m.hoogreef@tudelft.nl, AIAA Member

I. Introduction

In recent years, the drive to meet aggressive emission reduction targets set for aviation [1], together with technological advancements in the field of power electronics, has fostered research on hybrid-electric aircraft. These configurations utilize electric power for some or all of their propulsive needs. In particular, such powertrain architectures can leverage on the favorable down-scaling of electrical systems to distribute smaller propulsion components along the airframe, in order to benefit from airframe-propeller aerodynamic synergies. The resulting Distributed Hybrid Electric Propulsion (DHEP) aims to improve the aero-propulsive efficiency of the aircraft. The Hybrid Electric Propulsion (HEP) in general may also be able to provide enhancements in powertrain efficiency. Recent studies have underscored the difficulty to translate theoretical benefits at subsystem level into aircraft-level improvements, whether it concerns the first [2] or second [3] of the two aforementioned objectives. Another interesting prospect of DHEP concerns the capability to increase the maximum lift coefficient through aero-propulsive interaction or by means of thrust-vectoring, which in turn can permit a higher wing loading.

The development of Hybrid Electric Aircraft (HEA) is a challenge in many ways: from a aircraft design viewpoint but also for the energy supply chain and for airport infrastructures. Regarding the latest, the adaptation of ground operations and of small infrastructures seems feasible, but not the complete reconstruction of airport gates and runways. In that context, it is assumed for this study that current gate size standards will not change by the eventual introduction of HEA. The span constraint can be particularly constraining for some categories of aircraft. For instance, Short-Medium Range (SMR) aircraft, which were responsible of more than half of aviation's CO2 emissions in 2019 [4] are particularly exposed to this span constraint. Indeed, the Airbus A320 family and Boeing 737 series exhibit rather similar wingspan at 35.8 m and 35.9 m for the A320NEO and 737MAX respectively, just short of the 36 m upper limit of code C gates, following standards from the International Civil Aviation Organization (ICAO). The use of more sophisticated wing-tip geometries over the years, from conventional on the 737 NG to intricate split-winglets on the 737MAX in a context of increasing Maximum Take-Off Mass (MTOM), reflects how this span constraint stimulates design innovations in order to reduce vortex drag.

The most popular aircraft from the smaller Regional class are not exposed to that span constraint: the wings of ATR-42 and -72 span over 24.6 and 27 meters respectively and that of the Dash 8-Q400 at 28.4 meters. None of those aircraft fit within the 24 meters upper span limit of ICAO code B gates, but all are far below the 36 meters limit of code C gates. However, the electrification of Regional aircraft would drive their MTOM higher and increase their wingspan, as underlined by various preliminary studies [5, 6]. One illustration of that trend can be observed with the design showcased by *Heart Aerospace* for the ES-30 aircraft. Even though the proposed payload and range are both below that of the ATR-42 (200 km full-electric range at 30 passenger capacity against 1555 km range at 48 passenger capacity), the wingspan of the ES-30, at 30.8 meters*, is significantly larger than the 24.6 meters of the ATR-42.

The present paper proposes to investigate how the 36 meters span limit affects the sizing of battery-powered HEA in the regional class. Furthermore, an increase in feasible wing loading may be particularly beneficial to aircraft which wingspan is limited by airport gate constraints by allowing an increase in MTOM without sacrificing in wing aspect ratio. Section III investigates the sensitivity of the sizing of a serial HEA aircraft serial to an increase in the Degree of Hybridization (DoH). Section IV repeats that investigation for the same aircraft configuration but equipped with a Leading Edge Distributed Propulsion (LEDP). For the remainder of this paper, the conventional aircraft that serves as the baseline for comparison will be called 'REG-baseline', while the HEA will be respectively called REG-serial and REG-serial-LEDP.

II. Aircraft Sizing Approach

The tool used for the preliminary sizing of the HEP aircraft considered in this study is an Aircraft Design Initiator (or simply *Initiator*), which has been developed in-house at TUDelft [7]. This software, which was initially conceived for the conceptual design of both conventional and unconventional aircraft configurations (eg: blended wing body and box-wing) has been modified in recent years to enable the analysis of HEP aircraft fitted with various DHEP layouts. It consists overall in successive convergence loops on MTOM, nested within each other and of increasing analysis fidelity, which iteratively alter high-level design variables to eventually converge towards an aircraft design that abides by the given set of input TLARs. Figure 1 shows the process at an aggregated level.

Powertrain modelling as well as aero-propulsive interactions are accounted for in the Class I iterative process, via a

*FlightGlobal, *Heart details dimensions of ES-30 as Swedish start-up pushes ahead with 30-seater*, September 2022, https://www.flightglobal.com/airframers/heart-details-dimensions-of-es-30-as-swedish-start-up-pushes-ahead-with-30-seater/150231.article

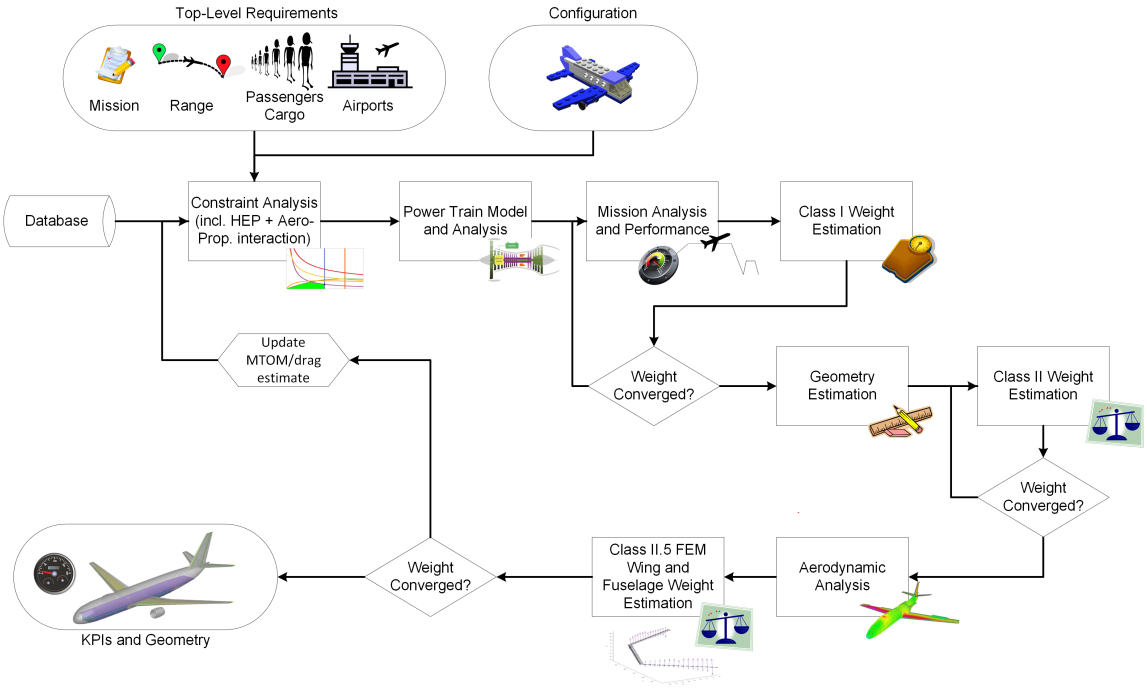

Fig. 1 Illustration of the *Initiator* process flow, for the design of hybrid electric aircraft, from [8]

generic sizing method suited especially for hybrid-electric aircraft with distributed propulsion [5].

For the power and wing sizing, a design selection diagram is produced for each component of the powertrain. A set of so-called *Power Control Parameters* (PCP), see Section II.B, define the relative power split within the powertrain and can be different from one constraint to the other. For each constraint of the selection diagram, a system of equation is solved, comprised of equations of motion and power distribution equations. Equations of motion are solved to find a flight equilibrium at the prescribed conditions of the constraint, with a specific aspect being the integration of various aero-propulsive models that alter the aero-propulsive characteristics of the aircraft and affect the performance constraints and the resulting feasible design space. The power split equations are also solved to compute the power distribution that corresponds to the aforementioned flight equilibrium. The resulting design selection diagram can therefore be established for each component of the powertrain such that the impact of the selection of a design point on the component sizing can be straightforwardly assessed. The design point is not selected by an optimizer, but rather is an a-priori design choice informed by engineering know-how.

The sizing of energy carriers (battery, fuel) are subsequently obtained from a Mission Analysis module that runs an integration scheme on the equations of motion of a point-mass aircraft along each flight phase to compute the respective energy needs. Once again, the PCP can be adapted for each phase of the mission and the aero-propulsive interactions are accounted for. The ClassI iteration starts with a design point in terms of wing loading and power loading for each component. It then iterates on the Take-off Mass (TOM), by recomputing each time the energy needed and therefore the mass of the energy carriers from the mission analysis, and by adapting the sizing and mass of the wing as well as of the power-related components to the TOM being evaluated.

A. System-level modeling

The system of power distribution equations and its resolution can be made generic to all hybrid powertrain architecture, composed of a "primary" powertrain which gathers all components that are mechanically linked to the Gas Turbine (GT) and of a "secondary" powertrain which includes components of the electrically-driven propulsion system. The modeling of each powertrain is based on the simplified conceptual representation of components and power flows. One significant assumption is that the GT power output is composed of the mechanical power on its shaft only, such that the GT core itself does not provide any propulsive power. If that assumption is quite erroneous for turbofan designs, where the core provides a non-negligible fraction of the thrust, it however holds for turbo-propeller or turbo-shaft

architectures. Powertrain components are not modeled, but rather have their properties a-priori assumed. This allows to reduce the computational time and provides the ability to directly control key-governing variables. The GT performance is not explicitly modeled; instead, a maximum thermal efficiency is assumed for the GT, which is down-rated by a lapse function which depends on the throttle setting and Mach number. Therefore the impact of operating conditions and eventual power off-take on GT performance is accounted for in a simplistic way within the *Initiator*. The *Initiator* is able to account for the aero-propulsive interactions of a large variety of propulsion layouts via several available low-fidelity aero-propulsive models. In the present study, the so-called 'LEDP' model used is an analytical model that was developed by de Vries et al. [5]. The sizing of the fuselage and of the wing primary structure is done within the Class 2.5 loop of the *Initiator*, via simplified finite-element methods. Concerning the wing, load cases account for the discrete loads of engine and wing-mounted components but not for aero-propulsive interactions, such that the aerodynamic loads are that of a 'clean' wing, without any propeller interaction. This approximation was shown to be acceptable [9] with only a minor impact on wing mass (below 1%). Overall, the *Initiator* should not be comprehended as a tool for the quantitative estimation of KPIs. But it is suited to rapidly produce aircraft designs and explore relative trends between different design. As such, the performance metrics of resulting hybrid-electric aircraft designs should be analyzed relatively to their baseline counterparts: aircraft designs obtained with the same methodology subject to the same TLARs, but with a conventional combination of powertrain and propulsion layout.

B. Power control parameters

Depending on the powertrain architecture, up to three so-called *power control parameters* (PCP), defined in Equations 1, 2 and 3 below, can be necessary to determine the power flow within each component. The *supplied power ratio*, see [2, 10], is expressed as the ratio of battery supplied power to the total supplied power.

$$\Phi = \frac{P_{bat}}{P_{bat} + P_f} \tag{1}$$

The second power control parameter is the *shaft power ratio*, defined as the ratio of the mechanical shaft power supplied to the secondary propulsion layout to the total shaft power produced by the powertrain.

$$\varphi = \frac{P_{s2}}{P_{s1} + P_{s2}} \tag{2}$$

Finally, the *gas turbine throttle* parameter, expressed in Equation 3 represents the power fraction at which the GT is operating, as the ratio of produced power to the maximum power it can produce in the given flight condition.

$$\xi = \frac{P_{GT}}{P_{GTmax}} \tag{3}$$

C. Requirements and configuration

Rather than compromising on payload-range capabilities to make a full electric aircraft fit within the span limit, it is chosen to select the Top Level Aircraft Requirements (TLARs) of the ATR-42 and adapt the Degree of Hybridization (DoH) to test the span constraint. Another justification to that choice is that the DoH selected for the harmonic mission would represent the lowest DoH of any mission from the payload range diagram. Indeed, any mission less restrictive than the harmonic one in terms of payload and/or range can be flown with the same battery but less fuel. This approach seems more oriented towards the overall objective of de-carbonation of aviation than the one that sets a limited range for full-electric operations (DoH of 1) with a range extension by burning fuel. The set of TLARs selected for the present study is summarized in table 1.

A serial architecture was selected to enable LEDP, without the range limitations typically imposed by fully-electric configurations. While previous work has shown that serial powertrains typically entail a significant powertrain weight penalty [6], this drawback may be offset if it enables a higher wing loading by means of LEDP. Furthermore, for high degrees-of-hybridization, a high amount of battery energy may enable low-emission or emission-free operation on missions with a shorter range than the design range.

It was purposely decided not to deviate from a conventional aircraft configuration apart from elements of hybridization. Some common elements of configuration for all aircraft sized in the present study are detailed in table 2. Most are inspired from the design of the ATR-42. However, in anticipation of a large increase in tail area the abreast seating is changed from 2-2 to 2-1 in order to lengthen the tail arms and the Vertical Tail (VT) sweep angle is increased to

30 degrees. The size of tails are obtained via a volume coefficient approach, with the coefficients values in table 2. Finally, an important aspect concerns the location of the energy carriers, which are located within the wing internal volume. Besides, for all aircraft considered in this study, unless specified differently, the selected design point (cf Section II) is based on the criteria of maximum wing loading. This design point generally produces the lowest MTOM for conventional aircraft [11] and also minimize MTOM for radical aircraft [2]. The sizing of HEA is highly sensitive to the underlying technology assumptions made; values used for all HEA in this study are listed in table 3.

D. Key Performance Indicators (KPIs)

The aircraft-level KPIs that are being monitored along the sensitivity analysis are listed below:

- E_{bat}: battery energy consumed along the nominal mission, excluding loiter and diversion.
- E_f: fuel energy consumed along the nominal mission, excluding loiter and diversion. It is representative of the CO2 emitted by the aircraft to complete its mission.
- DoH: Degree of Hybridization, defined in equation 4 . It is computed with respect to the energy spent during the nominal mission, excluding loiter and diversion.
- $PREE$: Payload Range Energy Efficiency, see equation 5, with PL the payload mass, R the mission range. The $PREE$ is computed with respect to the energy spent during the nominal mission, excluding loiter and diversion.

$$DoH = \frac{E_{bat}}{E_{bat} + E_f} \tag{4}$$

$$PREE = \frac{PL.R}{E_{bat} + E_f} \tag{5}$$

Table 1 Top Level Aircraft Requirements (TLARs) that apply to all for aircraft in this study.

Spec.	Unit	Required Value	Condition
Passenger capacity	-	48	@ 30" pitch
Maximum payload	kg	5450	
Harmonic range	nmi	500	
Cruise Mach number	-	0.4	
Cruise altitude	ft	23000	@ ISA
Landing distance	m	1006	@ SL, ISA
Takeoff distance	m	1372	@ SL, ISA
Diversion range	nmi	100	
Diversion Mach number	-	0.2785	
Diversion altitude	ft	4920	@ ISA
Time-to-Climb	min	22	after T/O @ MTOM, to cruise conditions

Table 2 Aircraft design parameters selected for all aircraft in the present study.

Design Parameter	Unit	Value
Abreast seating	-	2 - 1
Wing aspect ratio	-	12
Wing taper ratio	-	0.47
Span-wise kink location	%	31.5
Thickness-to-chord ratio	%	[18, 16, 13] @ [root, kink, tip]
Horizontal tail volume coefficient	-	1.00
Vertical tail volume coefficient	-	0.08
Vertical tail sweep	deg	30
Battery location	nmi	wing
Fuel tank location	-	wing

Table 3 Hypothetical technology assumptions for electric powertrain components.

Parameter	Unit	Value	Remark
Battery gravimetric energy density	Wh/kg	380	pack-level
Battery gravimetric power density	W/kg	2000	pack-level
Battery volumetric mass density	kg/m^3	1750	pack-level
Battery volumetric energy density	Wh/lt	665	pack-level, obtained from above properties
Battery minimum state-of-charge	%	20	
Electromotors gravimetric power density	W/kg	4000	includes TMS, controllers and converters

III. Sizing of HEA of conventional propulsion layout

In the selected serial configuration, see fig. 2a and fig. 2b, called REG-serial, two wing-mounted gas turbines see a 100% power off-take towards the electric powertrain via a gear box. The four wing-mounted propellers are therefore driven by electric motors.

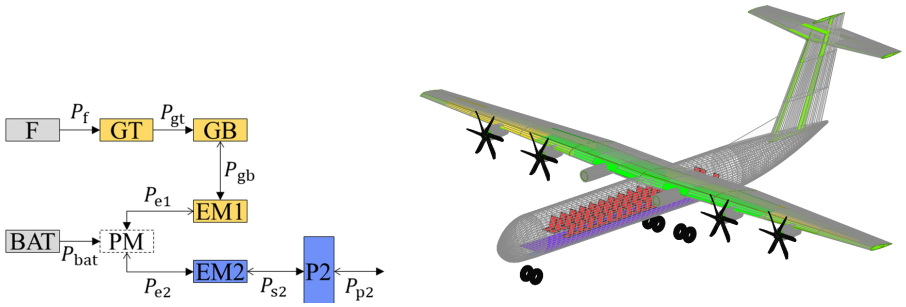

(a) Serial powertrain **(b) REG-serial**

Fig. 2 Isometric representation of the REG-serial configuration together with the notional representation of its powertrain architecture.

For the power-control strategy, two scenarios were considered. In the first, the battery was sized to provide the power required for cruise, to limit the battery power output. In the second, the gas turbine was sized to provide cruise power, to increase the gas turbine power loading and have the gas turbine perform near its peak efficiency during cruise. Exploratory analyses showed a clear advantage in terms of roughly +30% PREE on the harmonic mission for the second strategy, and therefore it was selected for the rest of the study. Figure 3 displays how the cruise constraint is sizing the GT but not the battery. In this case, the battery supply power ratio Φ is adapted for all constraints (but cruise obviously), to shift them towards higher power loading values in the GT constraint diagram until the cruise constraint becomes active.

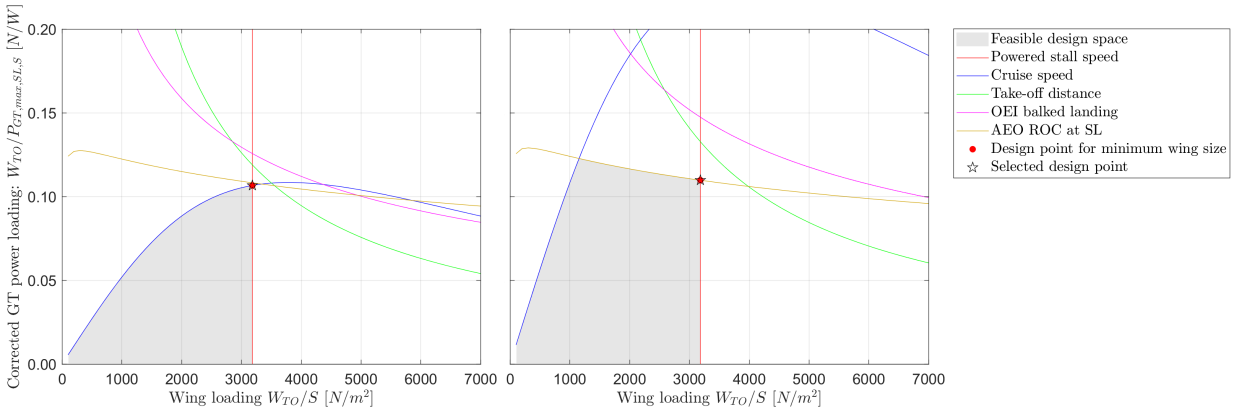

(a) **(b)**

Fig. 3 Component constraint diagrams of the gas turbine (a) and the battery (b) for the REG-serial configuration.

In order to limit the battery size and optimize the DoH for the nominal mission only, the battery supplied power ratio is kept null during segments of the diversion mission and loiter for as long as the GT is powerfull enough to cover those flight phases, which stops being the case for large supplied power ratio that entail relatively smaller gas turbines. Besides, during descent the GT are maintained at idle throttle (3%) while the battery supply power is shut. The GT must remain switched on until the end of descent, in the eventuality of a balked landing, for which the battery alone can not provide the required propulsive power.

Figure 4 shows how the DoH varies linearly with Φ_{cruise}, being nearly equal in value, since the fraction of energy required from the batteries to perform the mission is governed by the power split in cruise. A first observation (top-right

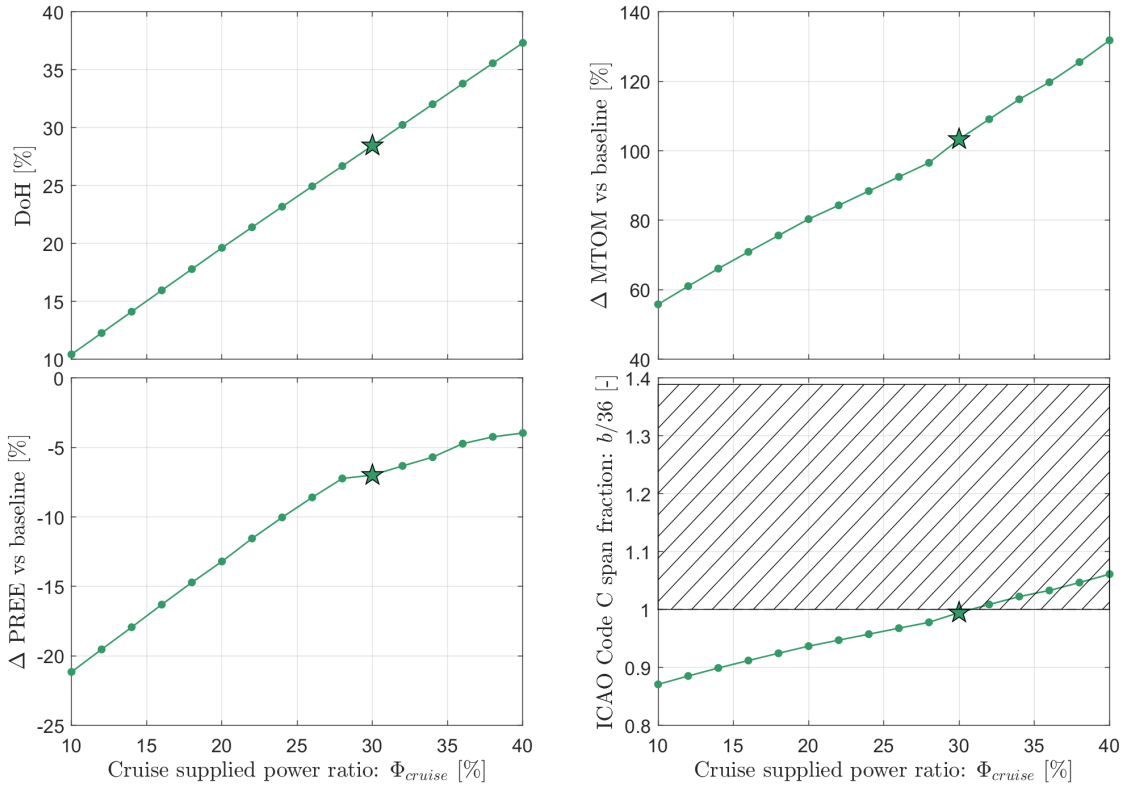

Fig. 4 Evolution of key design and performance parameters with increasing Φ_{cruise} for the REG-serial aircraft configuration.

plot of Fig. 4) concerning the MTOM is that even for the lowest value in supplied power ratio, the MTOM increase over the REG-baseline aircraft exceeds 50%, which has more to do with power conversion losses from the gas turbine than the added mass of the battery. The rate of increase of MTOM with slightly lowers until $\Phi_{cruise} = 0.28$, from which the trend gets pseudo-linear with a much larger rate of increase. This change of trend is driven by the evolution in fuselage mass, which sees the impact of larger aero-surfaces and their associated aerodynamic loads on the fuselage structural weight.

The PREE exhibits a pseudo linear trend up to the same $\Phi_{cruise} = 0.28$ threshold and then starts a much less pronounced increase, which outlines the high sensitivity of the PREE to the MTOM. The reason behind the increase in PREE with Φ_{cruise} can only be related to the larger fraction of energy that channels through the electric powertrain of higher efficiency. It is un-surprising that lower values of Φ_{cruise} exhibit a large PREE penalty with respect to the baseline, as they get closer to the point ($\Phi_{cruise} = 0$) where 100% of the propulsive power suffers from power conversion losses. Finally, the wing span is proportional to the root square of the MTOM, as the wing loading is unaffected by the battery supplied power ratio. The last value of battery supplied power ratio for which the 36 m upper span limit remains inactive is $\Phi_{cruise} = 0.30$, which incidentally in the present case, almost corresponds with the upper limit for the linear increase in PREE. Results presented subsequently for the REG-serial aircraft correspond to the one sized for $\Phi_{cruise} = 0.30$, represented by a star in Fig. 4.

The increase in aerodynamic surfaces is well depicted by Fig. 5, with the wing area roughly doubled (34.7 m^2 vs 17.1 m^2).It can be seen that the overall aircraft length is also altered to some extend via the increase in tail size.

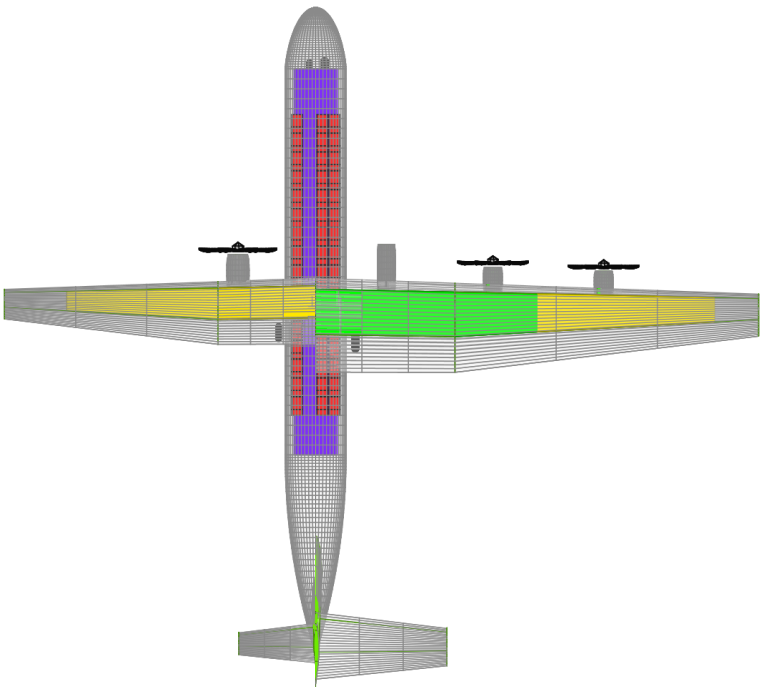

(a) REG-baseline **(b) REG-serial**

Fig. 5 Side-by-side top representations to scale of the left-hand half of the REG-baseline aircraft and the right-hand half of the REG-serial aircraft (Φ_{cruise} = 0.30). Energy carriers are located within the main wing spars, the fuel in yellow while the battery is displayed in green.

Table 4 has more details about the comparison between REG-baseline aircraft ad the selected REG-serial. A first remark is that the MTOM of the REG-baseline is 8% lower than that of the ATR-42. This could be explained by the higher fuselage slenderness ratio, but also by a smaller tail size. For the REG-serial, the presence of the battery to downscale the GT sizing to the cruise power requirement manages to triple the GT power loading. Yet the MTOM is doubled, such that overall the GT is only one third smaller than the one that equips the REG-baseline. Besides, the nearly 12 tons of battery itself largely overcome the GT weight reduction. Even though the MTOM of the REG-serial is twice as large as that of the REG-serial, its PREE deficit is limited to 7%, which is permitted by the high efficiency of the electric powertrain. Despite this reduction in overall energy efficiency, the DoH of 28.4% permits fuel burn savings of 23%.

Table 4 Comparison between REG-baseline and the REG-serial (Φ_{cruise} = 0.30).

	Unit	REG-baseline	REG-serial	
			value	Δ [%]
Design selection variables				
Φ_{cruise}	–	0	0.30	N.A.
GT power loading $W_{TO}/P_{GT,max,SL}$	N/W	0.054	0.16	+ 205
Battery power loading W_{TO}/P_{bat}	N/W	N.A.	0.103	N.A.
Takeoff wing loading W_{TO}/S_w	kN/m^2	3.18	3.18	0.0
Masses and dimensions				
MTOM	tons	17.1	34.7	+ 103
OEM (excluding battery)	tons	10.3	17.4	+ 69
Fuel mass (on takeoff)	tons	1.35	1.30	-3.8
Battery mass	tons	0	11.6	N.A.
Wing span	m	25.1	35.8	+ 42
Wing area	m^2	52.7	106.8	+ 103
KPIs on nominal mission				
Degree of hybridization	–	0	28.4	N.A.
Fuel energy consumption	GJ	38.2	29.4	-23.1
Electric energy consumption	GJ	0	11.7	N.A.
PREE	–	1.30	1.21	- 7

IV. Sizing of HEA with higher wing loading via LEDP

In this section, the REG-serial configuration is modified to accommodate a LEDP layout with the objective to push the 36 m span limit towards higher values of DoH, via an increase in wing loading. In this case, the aerodynamic interaction effects between propeller and wing are exploited to enhance the effective maximum lift coefficient, and thereby increase the allowable wing loading. This is only possible if the lift enhancement is guaranteed in the worst-case scenario. This strategy is therefore only viable if numerous propellers are employed, such that a substantial lift enhancement remains if one or more propellers fail. Therefore, a LEDP configuration with 10 propellers covering 74% of the span was selected, positioned such that the outboard propeller does not extend beyond the wingtip, as shown in Fig. 10. Compared to the previous configuration, REG-serial, the higher number of propellers implies a lower diameter, which is also required for ground clearance near the wing tip.

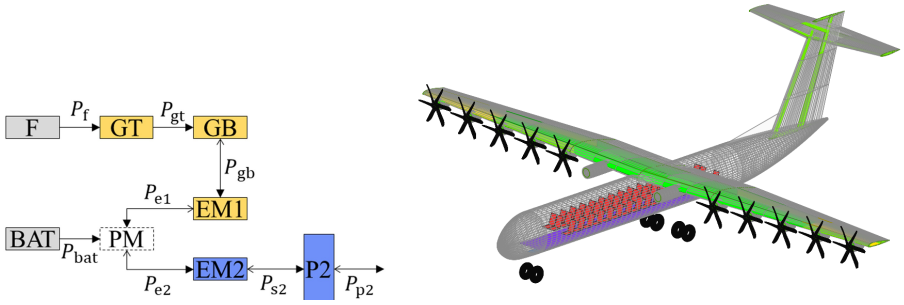

(a) Serial powertrain **(b) REG-serial-LEDP**

Fig. 6 Isometric representation of the REG-serial-LEDP configuration (b) together with the notional representation of its powertrain architecture (a).

The first sizing attempts at maximum wing loading did not produce feasible designs because the battery and fuel could not fit within the available internal wing volume, delimited between the two main spars. A quick scaling analysis

reveals indeed that the wing span scales with $S^{1/3}$, while the wing volume scale with $S^{2/3}$, such that the wing internal volume scales down faster than the wing span when the allowable wing loading is increased at constant takeoff weight. in other words, by trying to mitigate the wing span constraint, the internal volume constraint was hit earlier. The wing loading was then lowered by selecting a design point manually, as outlined by Fig. 7, such that overall a sizing with a wing loading increased over that of the REG-serial but still able to host battery and fuel within its wing internal volume was found. Φ_{cruise} was varied identically as in the previous section. The upper value in Φ_{cruise} was increased from 0.40 to 0.50. High-level sensitivity results of the REG-serial-LEDP are summarized in Fig. 8, in comparison with those obtained for the REG-serial. The DoH varies identically with Φ_{cruise} as explained before.

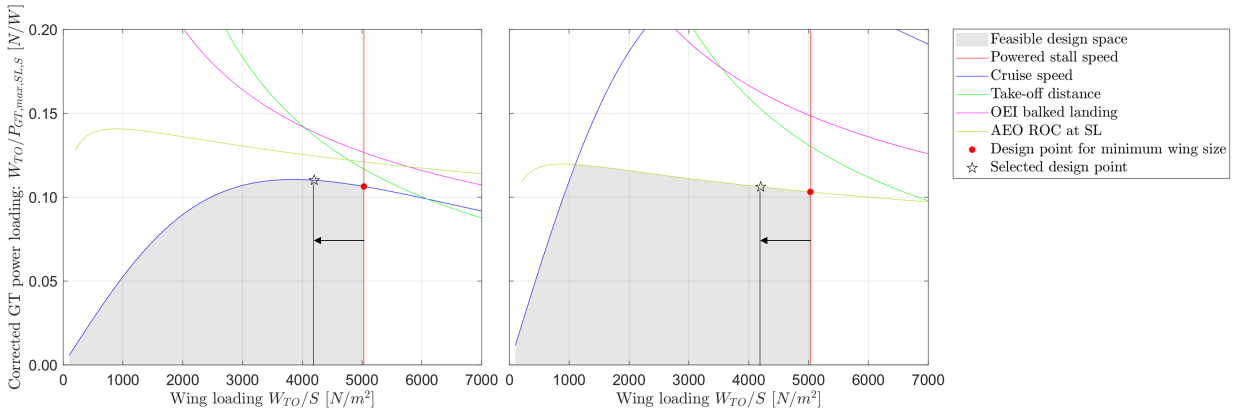

(a) **(b)**

Fig. 7 Component constraint diagrams of the gas turbine (a) and the battery (b) for the REG-serial-LEDP configuration. The selected design point is shifted towards lower wing loading compared to the point of maximum wing loading.

For one condition, $\Phi_{cruise} = 0.36$, the design loop failed to converge numerically. The REG-serial-LEDP exhibits a slight reduction in MTOM compared to the REG-serial at a given value in battery supplied power ratio in cruise. This can be explained by the lower wing area together with the lower tail area that follows immediately via the volume coefficient approach. Identically to the REG-serial, a same change in trend can be observed on the MTOM variation with Φ_{cruise}, the rate of increase getting more pronounced for higher values of battery supplied power ratio. Some change in the topology of the fuselage and wing structure can explain such sudden change in behavior.

The PREE of the REG-serial-LEDP is slightly higher than that of the REG-serial for values of $\Phi_{cruise} < 0.24$. But the PREE evolution for the REG-serial-LEDP then flattens out to eventually start decreasing past $\Phi_{cruise} = 0.40$. At this point, the MTOM of both serial configurations are identical, however the PREE of the REG-serial is higher, which suggests a higher aero-propulsive efficiency and /or a higher powertrain efficiency. It should be noted at this point that for the REG-serial-LEDP , a fixed fraction (0.835) of the maximum feasible wing loading is assumed when shifting the design point manually (see Fig. 7). However the maximum allowable wing loading changes slightly with each Φ_{cruise} because the drag polar is modified between each case. Indeed, the progressive increase in MTOM requires a larger wing, while the fuselage remains identical. The required thrust during landing is therefore different, which affects the increase in lift enabled the LEDP layout and consequently alters the maximum allowable wing loading. The wing loading values actually selected for the REG-serial-LEDP range from 3.741 kN/m^2 ($\Phi_{cruise} = 0.10$) to 3.718 kN/m^2 ($\Phi_{cruise} = 0.50$).

Incidentally, the $\Phi_{cruise} = 0.40$ of maximum PREE is also the last value that enables to fit within the 36 meters span constraint: it represents a compromise in the current case and the aircraft sized for $\Phi_{cruise} = 0.40$ is selected to represent the REG-serial-LEDP configuration, represented by an orange star in Fig. 8.

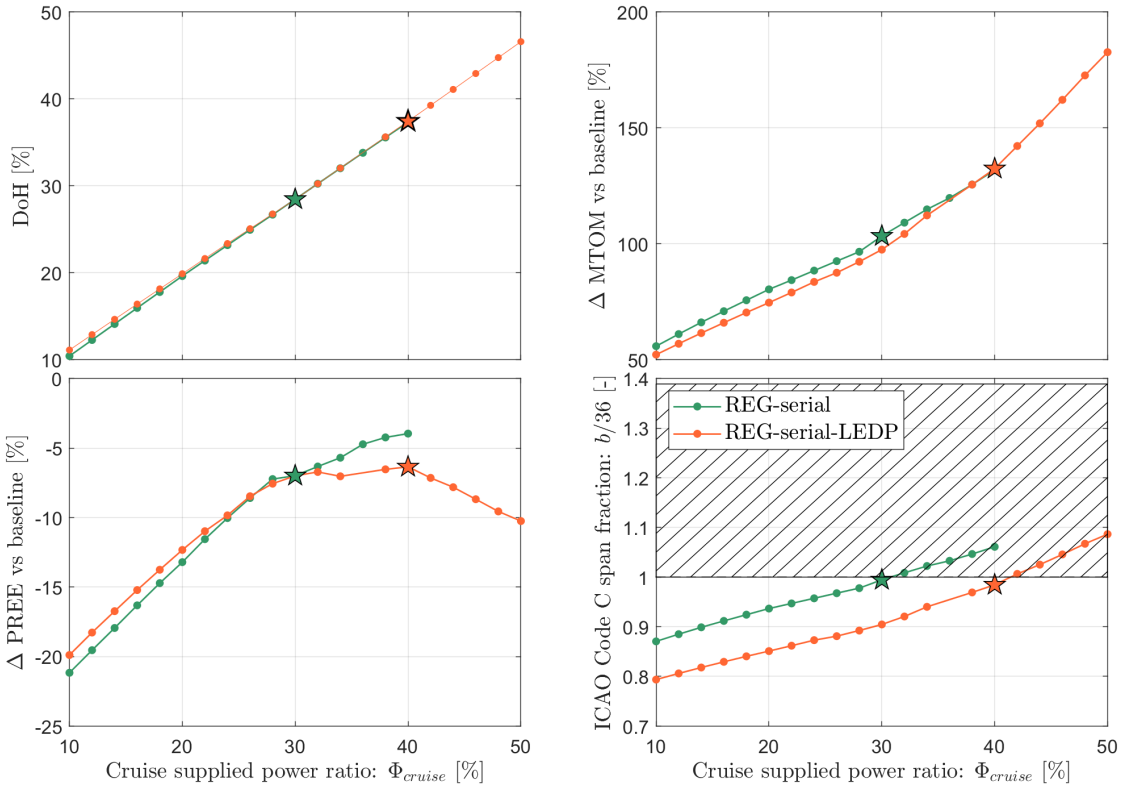

Fig. 8 Evolution of key design and performance parameters with increasing Φ_{cruise} for the REG-serial aircraft configuration and the REG-serial-LEDP.

Figure 9 and Fig. 10 outline the different in size obtained between the REG-baseline and the selected REG-serial-LEDP. The size of the REG-serial-LEDP is almost strictly identical to the REG-serial, only for a higher Φ_{cruise}. It is shown here that the LEDP approach succeeds in pushing the feasible DoH higher. Table 5 summarizes results for both serial aircraft and their relative variations with respect to the baseline aircraft. By shifting the design towards a higher wing loading, the GT power loading of the REG-serial-LEDP is increased even further compared to the increase already obtained with the REG-serial. The actual DoH achieved gets to 37.4 %, which in combination with a slightly better PREE, manages to lower the fuel consumption even further than achieved by the REG-serial: the fuel burn is a third lower than the REG-baseline. This is obtained at the price of an even higher MTOM, which is 2.3 times higher than that of the REG-baseline.

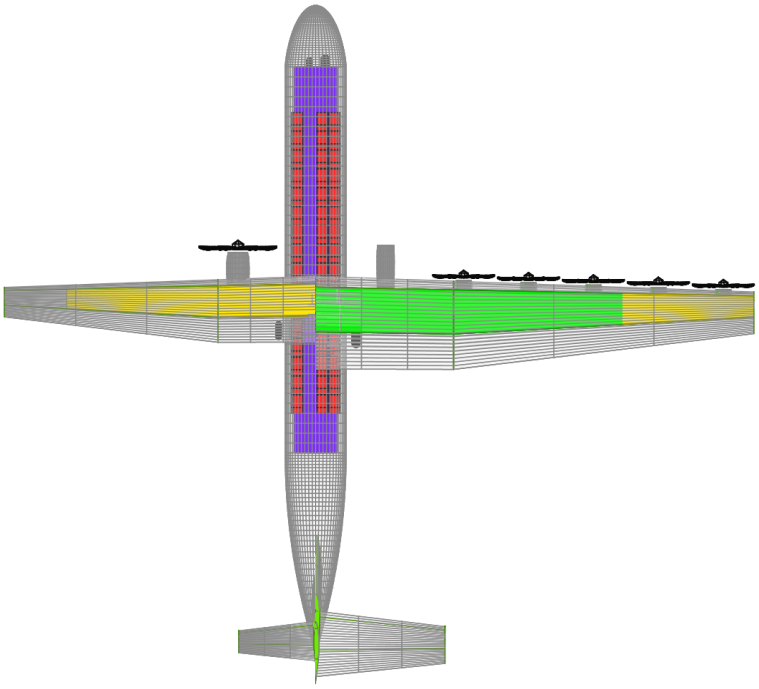

(a) REG-baseline **(b) REG-serial**

Fig. 9 Side-by-side top representations to scale of the left-hand half of the REG-baseline aircraft and the right-hand half of the REG-serial-LEDP aircraft selected for ($\Phi_{cruise} = 0.40$). Energy carriers are located within the main wing spars, the fuel in yellow while the battery is displayed in green.

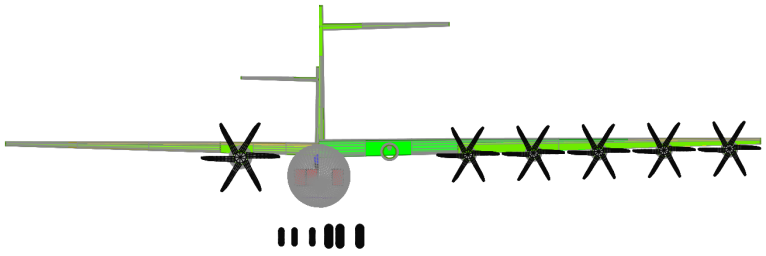

(a) REG-baseline **(b) REG-serial-LEDP**

Fig. 10 Side-by-side front representations to scale of the right-hand half of the REG-baseline aircraft (a) and the left-hand half of the REG-serial-LEDP aircraft selected for $\Phi_{cruise} = 0.40$ (b). The selected REG-serial has a wingspan of 35.4 meters. Energy carriers are located within the main wing spars, the fuel in yellow while the battery is displayed in green.

Table 5 Comparison between REG-baseline, REG-serial (Φ_{cruise} = 30) and REG-serial-LEDP (Φ_{cruise} = 40)

	unit	REG-baseline	REG-serial		REG-serial-LEDP	
			value	Δ [%]	value	Δ [%]
Design selection variables						
Φ_{cruise}	–	0	0.30	N.A.	0.40	N.A.
GT power loading $W_{TO}/P_{GT,max,SL}$	N/W	0.054	0.16	+ 205	0.23	+ 324
Battery power loading W_{TO}/P_{bat}	N/W	N.A.	0.103	N.A.	0.09	N.A.
Takeoff wing loading W_{TO}/S_w	kN/m^2	3.18	3.18	0.0	3.72	+ 17
Masses and dimensions						
MTOM	tons	17.1	34.7	+ 103	39.7	+ 132
OEM (excluding battery)	tons	10.3	17.4	+ 69	17.0	+ 65
Fuel mass (on takeoff)	tons	1.35	1.30	-3.8	1.23	-9.3
Battery mass	tons	0	11.6	N.A.	16.0	N.A.
Wing span	m	25.1	35.8	+ 42	35.4	+ 41
Wing area	m^2	52.7	106.8	+ 103	104.7	+ 99
KPIs on nominal mission						
Degree of hybridization	–	0	28.4	N.A.	37.4	N.A.
Fuel energy consumption	GJ	38.2	29.4	-23.1	25.5	-33.2
Electric energy consumption	GJ	0	11.7	N.A.	15.3	N.A.
PREE	–	1.30	1.21	- 7	1.21	- 6.4

Finally, to illustrate the impact of the volume constraint, Fig. 11 displays the ratio of required volume for energy carriers to available wing volume. This 'occupied volume fraction' varies with Φ_{cruise} for both the REG-serial and the REG-serial-LEDP. The first striking observation concerns the predominance of the battery volume over the fuel volume, even for smaller Φ_{cruise}. If it is well discussed and acknowledged in the aircraft community that the gravimetric energy density is a key technology parameter to improve to enable battery-assisted flight, it is less common to discuss about the criticality of the deficit in volumetric energy density of batteries compared to jet fuel. For a given Φ_{cruise}, the occupied volume fraction is higher for the REG-serial-LEDP due to the decreased wing volume associated to the increased wing loading. A local maximum in the occupied volume fraction is observed around Φ_{cruise} = 0.36, marked by a black diamond on Fig. 11, even though the curve is rather flat. Besides, even for the REG-serial-LEDP, there is still ample margin (about 40%) in the occupied volume fraction to increase further the wing loading and hence the DoH. That is because the volume constraint was evaluated on the first iteration of the Class1 loop, when the wing loading is higher that it becomes for subsequent iterations, such that the manually selected design point is accounting for a smaller wing volume than it eventually is. This current limitation does not affect the consistency of the obtained aircraft but leaves margin for a higher value in wing loading before the volume constraint is active. Future works will correct that and explore the trade-off between span constraint and volume constraint in more detail.

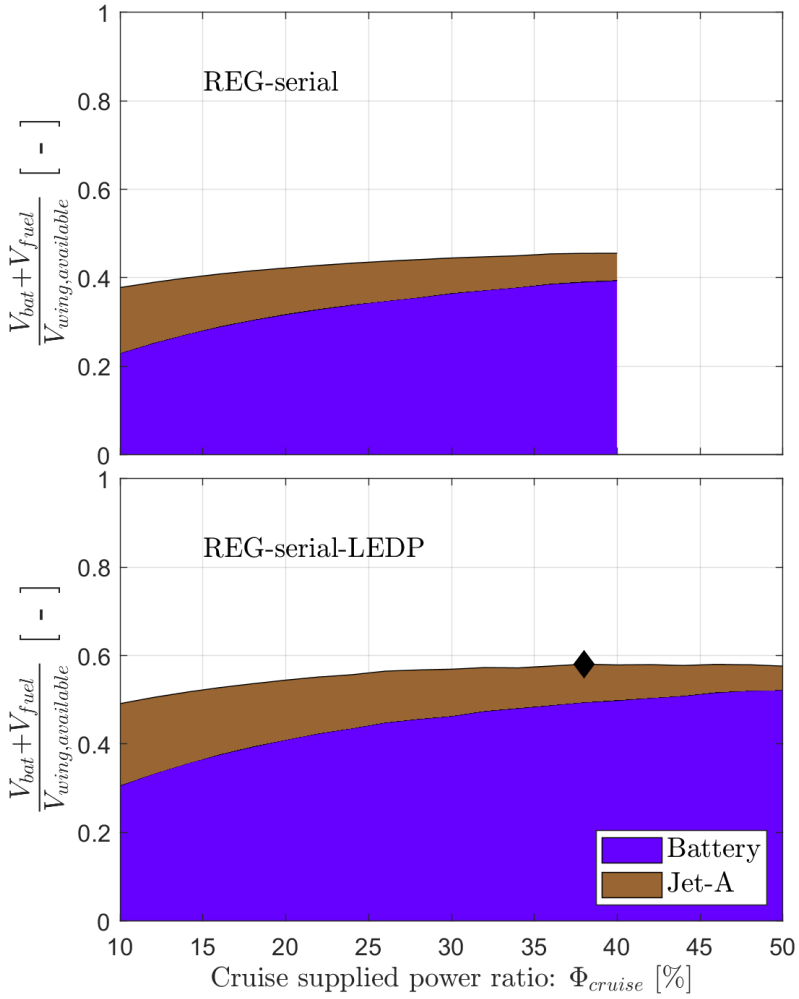

Fig. 11 Evolution of the ratio of required volume for the energy carriers to the available wing volume with increasing battery supplied power ratio in cruise Φ_{cruise}.

V. Discussions

A. Limitations

The results of Section III and Section IV show that serial HEA can significantly lower their fuel burn compared to a conventional aircraft for the same set of TLARs. However, these findings are exposed the following limitations:

- The battery sizing model used in this study is elementary and takes the highest of the two masses determined by battery power and energy requirements.
- The current sizing approach does not account for landing impact loads for the sizing of wing and fuselage.
- The tails are currently sized by a volume coefficient approach, where the coefficients are assumed constant for all aircraft and cases considered and values taken from conventional turboprop designs.
- The landing gear sizing and integration does not fully account for the requirements related to larger and heavier HEA.
- The relative benefits of the serial HEA configuration over a conventional design hinges on the efficiency superiority hold by the electric powertrain over the thermal one. Results are therefore highly sensitive to assumptions about the respective efficiencies of all components within the powertrain.

To overcome these limitations, future work should incorporate the sizing and integration of a battery TMS, that ideally accounts for all power requirements of different flight phases and is sized by the most constraining one. Landing impact loads should be accounted for in some ways, either by adding the corresponding load case to the Class2.5 sizing or by applying correction factors at lower fidelity. Tails should be sized by a stability analysis rather than based on volume coefficients. Landing gear sizing and integration should account for the effect of increased landing gear mass, increased landing gear volume as well as increased landing gear track width. Technology assumptions relative to power electronics should be closely monitored, but those relative to gas turbine performance are equally important.

B. General assumptions

The following assumptions are implicitly made for the current study:

- The increase in wing loading via LEDP hinges on the assumptions that powered stall speed can be accepted by certification standards. The presence of multiple leading edge-mounted engines is an argument that still must be confronted to the certification approach.
- A fuselage-mounted main undercarriage configuration is assumed for all aircraft in the present study. A different configuration, such as wing mounted, may have large implications.
- A high-wing configuration is assumed to maintain the boarding ease characteristic of high-wing aircraft. However, a low-wing configuration would probably be beneficial for the landing gear sizing and integration, where smaller distributed propellers can enable a lower landing gear strut length.

C. Implication of results

1. Wing volume constraint

If the increase in wing-loading is severely limited by the wing volume constraint, the former can be achieved by enhanced high-lift devices (leading-edge slats and trailing-edge flaps), which may add less weight and complexity than a LEDP layout. Besides, the occupied volume fraction would be quite sensitive to the thickness-to-chord ratio of the wing airfoil section used and to the wing planform. Rather thick sections are assumed in this study (see Table 2), but faster aircraft with thinner airfoils may be confronted to the occupied volume fraction constraint much sooner (for lower DoH) than in the present case. As such, the feasible wing loading should quite sensitive to cruise speed.

2. Landing gear sizing and integration

The HEA sized in the present study are likely to represent a specific challenge from a landing gear sizing and integration point of view. One obvious adverse trend concerns the increase in maximum landing mass. The landing mass fraction is assumed to be 1 in the present study: the maximum landing mass is therefore twice as high, or even greater, than the REG-baseline, such that all landing gear structures are significantly heavier and more voluminous. Fuselage fairings that host the landing gear would need to become significantly more voluminous, increasing fuselage drag. Besides, the landing mass more than doubles while the fuselage cross-section remains identical. That calls for a significant strengthening of the fuselage to account for landing impact loads. Finally, another adverse scaling

trend concerns the ratio of landing gear track width to aircraft wing span. While the wing span is 42% larger than the REG-baseline, the track width of the main undercarriage can not be increased much beyond the fuselage width.

3. Operational requirements

If the subsequently obtained HEA have such a larger footprint than the REG-baseline, their usage is probably restricted to large airport, where the available runway length is not as restrictive as stated in the initial requirements. Relaxing the take-off and landing distance requirements would significantly change the feasible DoH and design wing loading for a given maximum 36 meter span. Furthermore, the obtained HEA have a much larger main undercarriage than the REG-baseline, such that it may not allow boarding without airport air-stairs anymore. If that requirement becomes irrelevant, a low-wing configuration would probably be beneficial for the landing gear sizing and integration, where smaller distributed propellers can enable a lower landing gear strut length.

VI. Conclusions

In this study a regional hybrid-electric aircraft with a serial powertrain is sized with and without the aero-propulsive effects to demonstrate how they influence the limitation in wing size imposed by airport span constraints. The two aircraft are sized for a set of TLARs comparable to an ATR42 and are compared to a conventional configuration sized for the same mission. For the serial HEA of conventional propulsion layout REG-serial, the highest value of Phi_{cruise} that could be implemented without hitting the 36 m span limit was 0.30. For this REG-serial aircraft, the DoH reaches 28.4%, the MTOM is twice as high as that of the baseline aircraft, the GT power loading 3 times as high and the fuel burn over the nominal mission is reduced by 23%.

A serial powertrain architecture is used in combination with a LEDP propulsion layout to increase the wing loading and enable a higher DoH before hitting the span constraint. However, for the highest wing loading permitted by the LEDP layout, the wing volume constraint was not satisfied. This results to a scaling trend which sees the internal wing volume scales down faster than the wing span with a decrease in wing area and is exacerbated by the lower volumetric energy density of batteries compared to jet-fuel. The wing loading was subsequently lowered by selecting a different design point in the constraint diagram , such that a supplied power ratio of 0.50 could be achieved without violating the volume constraint. With the resulting wing loading value, 17% higher than for the REG-serial, the highest value of Phi_{cruise} that could be implemented without hitting the 36 m span limit was 0.40. For this REG-serial-LEDP aircraft, the DoH reaches 37.4%, the MTOM is 2.3 times as high as that of the baseline aircraft, the GT power loading 4.2 times as high and the fuel burn over the nominal mission is reduced by a third.

It was therefore shown that battery-assisted aircraft can offer a significant reduction in fuel burn by reaching a high enough combination of DoH and PREE. It was also shown that an increase in wing loading could be used to reach a higher feasible DoH before hitting the 36 meters span constraint, and that the PREE deficit to the baseline aircraft could be rather identical such that the fuel burn can be further reduced. However, the debilitating impact of battery mass on MTOM significantly alters the dimensions of the subsequently obtain HEA, in particular the relative dimensions of the wing with respect to the fuselage, to the point where additional hurdles must be considered. Some directly concern the aircraft design itself, such as the landing gear sizing and integration, others concern fundamental operational aspects, such as the relevance of field length requirements. Further work on those aspects would enable to identify limitations and opportunities for regional HEA.

Contact Author Email Address

You can contact the author at the following email address: v.o.bonnin@tudelft.nl

Copyright Statement

Acknowledgements

Research presented in this publication was performed under the CHYLA project. This project has received funding from the European Union's Horizon 2020 research and innovation programme under grant agreement No. 101007715. The authors would like to thank CHYLA project participants for joint work sessions on the preliminary down-selection of technological combinations.

References

[1] European Commission, Directorate-General for Mobility and Transport, Directorate-General for Research and Innovation, "Flightpath 2050: Europe's Vision for Aviation," Tech. rep., 2011. URL https://data.europa.eu/doi/10.2777/15458.

[2] de Vries, R., Hoogreef, M., and Vos, R., "Preliminary Sizing of a Hybrid-Electric Passenger Aircraft Featuring Over-the-Wing Distributed-Propulsion," *AIAA Scitech 2019 Forum*, 2019. doi:10.2514/6.2019-1811, URL https://arc.aiaa.org/doi/abs/10.2514/6.2019-1811.

[3] van Holsteijn, M. R., Gangoli Rao, A., and Yin, F., "Operating characteristics of an electrically assisted turbofan engine," *Turbo Expo: Power for Land, Sea, and Air*, Vol. 84058, American Society of Mechanical Engineers, 2020.

[4] Grayver, B., Rutherford, D., and Zheng, S., "CO2 Emissions from Commercial Aviation. 2013, 2018, and 2019," Tech. rep., International Council on Clean Transportation, 2020.

[5] de Vries, R., Brown, M., and Vos, R., "Preliminary Sizing Method for Hybrid-Electric Distributed-Propulsion Aircraft," *Journal of Aircraft*, Vol. 56, No. 6, 2019, pp. 2172–2188. doi:10.2514/1.C035388, URL https://doi.org/10.2514/1.C035388.

[6] Hoogreef, M., Vos, R., de Vries, R., and Veldhuis, L. L., "Conceptual Assessment of Hybrid Electric Aircraft with Distributed Propulsion and Boosted Turbofans," *AIAA Scitech 2019 Forum*, American Institute of Aeronautics and Astronautics, 2019. doi:10.2514/6.2019-1807.

[7] Elmendorp, R., Vos, R., and La Rocca, G., "A Conceptual Design and Analysis Method for Conventional and Unconventional Airplanes," *Proceedings of ICAS 2014*, 2014.

[8] Hoogreef, M., de Vries, R., Sinnige, T., and Vos, R., "Synthesis of Aero-Propulsive Interaction Studies Applied to Conceptual Hybrid-Electric Aircraft Design," *AIAA Scitech 2020 Forum*, 2020. doi:10.2514/6.2020-0503, URL https://arc.aiaa.org/doi/abs/10.2514/6.2020-0503.

[9] der Leer, Q. V., and Hoogreef, M., "Aero-Propulsive and Aero-Structural Design Integration of Turboprop Aircraft with Electric Wingtip-Mounted Propellers," *AIAA SCITECH 2022 Forum*, American Institute of Aeronautics and Astronautics, 2022. doi:10.2514/6.2022-0167.

[10] Isikveren, A., Kaiser, S., Pornet, C., and Vratny, P., "Pre-design strategies and sizing techniques for dual-energy aircraft," *Aircraft Engineering and Aerospace Technology*, Vol. 86, No. 6, 2014, pp. 525–542. doi:10.1108/aeat-08-2014-0122.

[11] Torenbeek, E., *Advanced Aircraft Design: Conceptual Design, Technology and Optimization of Subsonic Civil Airplanes*, Wiley, 2013.